Considerations with using unmanned aircraft systems in turfgrass

Dale J. Bremer, Kansas State University, USA; Dana G. Sullivan, TurfScout, LLC, USA; Phillip L. Vines, Rutgers, University of Georgia, USA, USA; David McCall, Virginia Polytechnic Institute and State University, USA; Jing Zhang, University of Georgia, USA; and Mu Hong, Colorado State University, USA

Abstract

In recent years, small unmanned aircraft systems (sUAS) and advancements in remote sensing technology have provided alternative and more affordable means for monitoring crop health and stress than ground-based (handheld or vehicle-mounted) or other aerial-based platforms (manned aircraft or satellites). However, few scientific studies have evaluated the application of sUAS in turfgrass systems. The use of sUAS in monitoring turfgrass requires an understanding of basic remote sensing principles; identifying the target of interest and the various sUAS platforms and sensors that provide the necessary resolution and frequencies to measure and monitor that target; calibration of sensors in the field; and data processing considerations. Those topics are discussed, followed by reviews of recent turfgrass field studies conducted to predict and manage drought stress and pest outbreaks and improve phenotyping capabilities in turfgrass breeding programs. The use of sUAS remote sensing in turfgrass offers unique possibilities and challenges, which are addressed herein.

Keywords: turfgrass; drones; small unmanned aircraft systems; unmanned aerial vehicles; remote sensing

1 Introduction

Remote sensing is the practice of obtaining information about an object without coming into physical contact with that object. Remote sensing-based observations have been the subject of agricultural research for well over 50 years, accompanied by significant advancements in foundational research and accessible technology. During that time, sensors have been deployed on platforms based on the ground (i.e., hand-held or vehicle-mounted) and in the air (i.e., manned aircraft or satellites). But in recent years, small unmanned aircraft systems (sUAS) have provided an alternative and more affordable means for remote data collection. Today, there are a wide variety of sUAS platforms ranging in size and operation (e.g., fixed-wing vs. multi-rotor). Along with the growing choice of platforms, more sensors (i.e., payloads) are becoming available representing a range in spatial and spectral resolutions.

2 Brief overview of light reflectance by plants

Irradiant solar energy can be reflected, absorbed, or transmitted by plants (Campbell, 1996). Plants absorb light used for photosynthesis, but a majority of the remaining light is reflected. Sensors typically measure the amount of light reflected by the plant canopy, and this provides an assessment of how well a plant utilizes solar energy for photosynthesis and growth. A typical spectral reflectance curve for green vegetation exhibits a small peak in the green region (~550 nm) of the spectrum followed by a sharp rise in the near-infrared (NIR) region (Figures 1 and 2). The NIR is primarily influenced by biomass production, canopy geometry, and subsequent light scattering (Hatfield et al., 2008, Sullivan et al., 2004), while the visible spectra are influenced by energy absorption for photosynthesis (Campbell, 1996). Plants with greater photosynthesis absorb more energy (i.e., reflect less) in the visible and may produce more biomass (affecting NIR reflectance) than their counterparts with lower photosynthesis, which typically results in different spectral reflectance response curves. Examples include turfgrass mown at different heights (Figure 1) and healthy vs. stressed turfgrass (Figure 2). The visible spectra generally exhibit a much smaller range in reflectance compared to the NIR. The small range within the visible region of "absorption" limits the visible region's sensitivity to plant stress. Examples of this limitation are often observed when applying normalized vegetation indices (discussed in section 2.1) that include visible spectra.

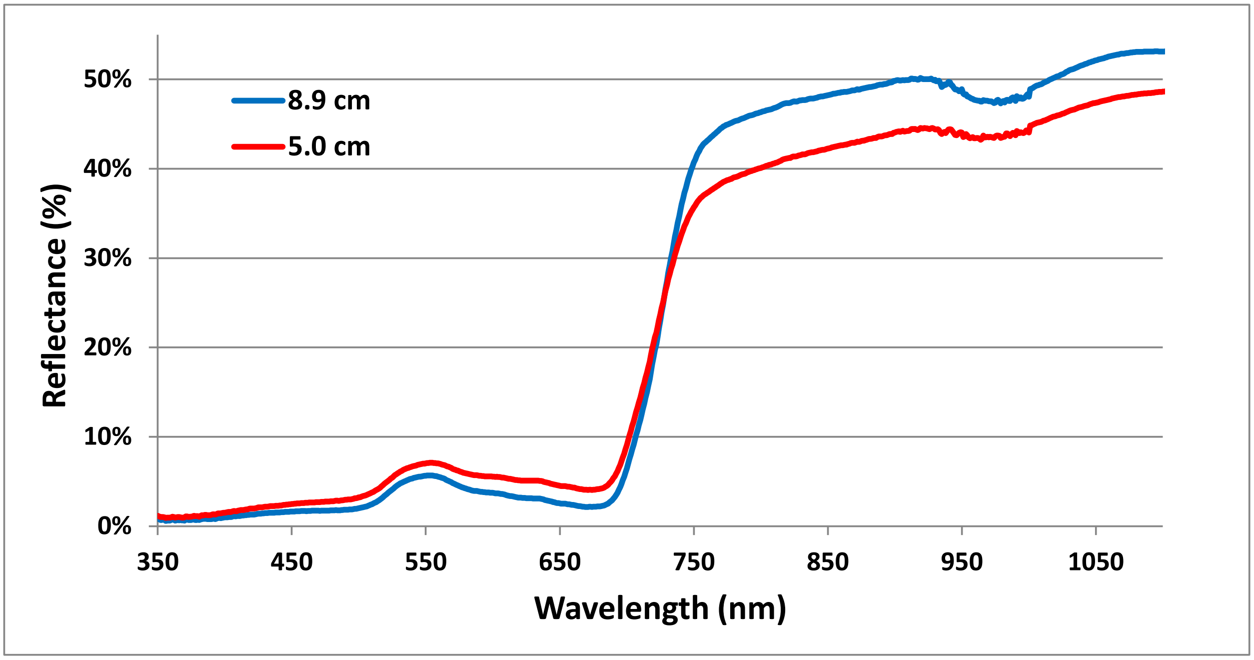

Figure 1. Spectral reflectance signatures of well-watered Kentucky bluegrass (*Poa pratensis* L.) turfgrass mown at two heights. Higher green leaf area index (LAI) at 8.9 cm (LAI=2.13) than 5.0 cm (LAI=1.28) resulted in lower reflectance in the visible (400-700 nm) and higher reflectance in the near infrared (NIR, >780 nm) at 8.9 cm. The dramatic rise in reflectance between approximately 690 and 750 nm is the "red edge". Reflectance was measured on 28 September 2010 with a portable spectroradiometer (FieldSpec 3, ASD, Boulder, CO, USA) at the Rocky Ford Turfgrass Research Center (Manhattan, KS, USA) (An et al., 2015).

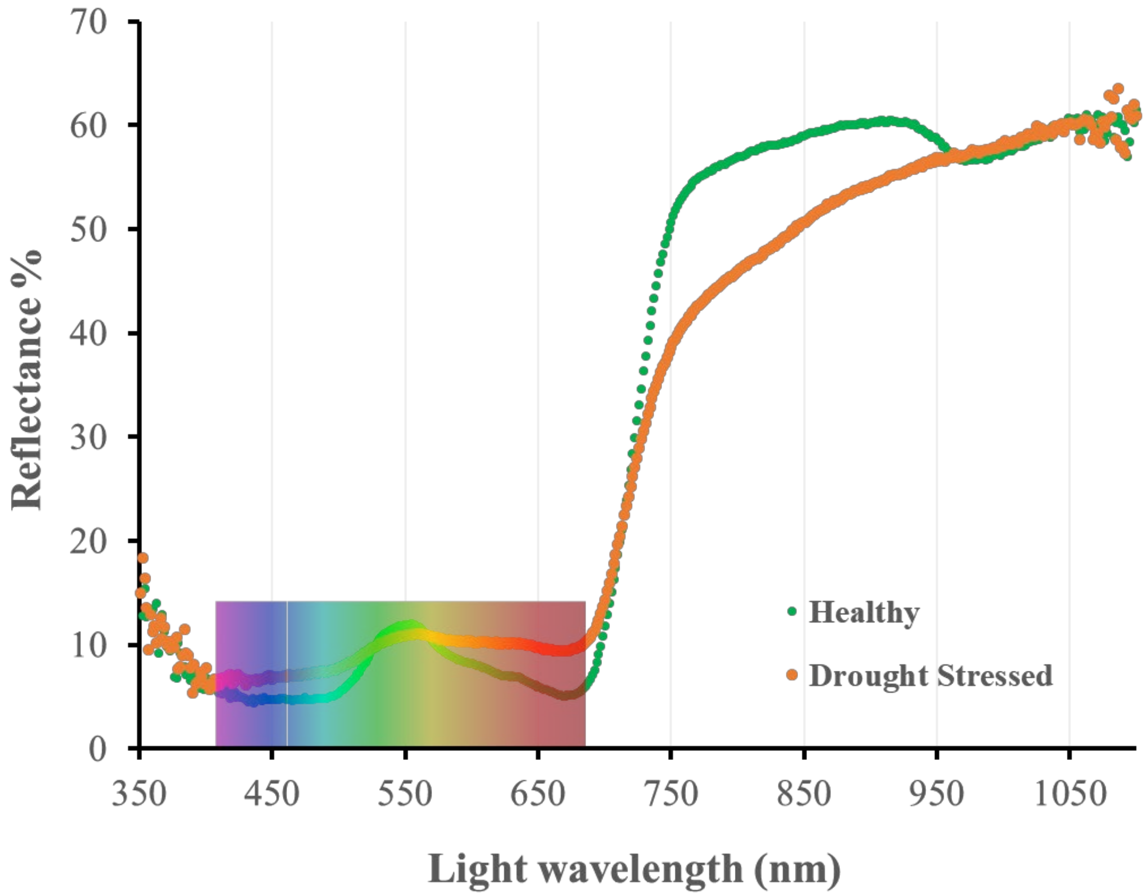

Figure 2. Spectral reflectance signatures of healthy and drought-stressed creeping bentgrass (*Agrostis stolonifera* L.) mowed at tee height (6.35 mm), measured with a portable spectroradiometer (PSR-1100F, Spectral Evolution, Haverhill, MA, USA) in a greenhouse study in Blacksburg, VA, USA. Reflectance is lower in the visible region of the spectrum (denoted by the colors corresponding to their respective wavelengths) because of absorption of energy by photosynthesis, compared with higher reflectance in the NIR (> ~750 nm). Figure by Travis Roberson.

2.1 Benefits and limitations of vegetation indices

Images are the base product or layer from which additional information can be derived. The most common data layers generated from remote sensing are vegetation indices (VIs), which are mathematical combinations of two or more spectral wavebands and are also referred to as radiometric indices. Vegetation indices are designed to target specific plant characteristics such as canopy geometry, chlorophyll content, nutrient status, or water demand to name a few

(Tucker, 1979; Sullivan et al., 2004, 2007; Gitelson et al., 2006). The earliest VIs were combinations of NIR and red band ratios with the specific intent to lessen the impact of variability in atmospheric conditions during the time of flight, as well as to separate the plant spectral response from the soil background (Hatfield et al., 2008). Specifically, VIs leveraged differences in soil and plant spectra to isolate plant spectral response prior to canopy closure in row crop agriculture. This was needed because early measurements were typically obtained via satellite imagery (30 m^2 pixel resolution or greater) or sensors aboard manned aircraft (1 m^2 per pixel resolution), which often resulted in a mixture of plant and soil within any one pixel (Sullivan et al., 2007). In more recent years, high resolution sUAS-based imaging has allowed practitioners to more easily segment images into plant and soil components for analysis.

One of the most well-known VIs, the normalized difference vegetation index (NDVI) (Rouse et al., 1974), is a normalized ratio of NIR and red spectral bands. The NDVI has been, in practice, a means to evaluate nitrogen and chlorophyll content, predict yields, and provide a measure of overall plant health status for more than five decades (Fenstermaker-Shaulis et al., 1997; Bell et al., 2004; Baghzouz et al., 2006, 2007; Sullivan and Holbrook, 2007; Caturegli et al., 2016, 2019). However, there are strengths and limitations associated with NDVI applications, particularly as applied to turfgrass. First, the NDVI is not linear with respect to plant response (Ritchie and Bednardz, 2005). The NDVI is a normalized measurement of NIR and red spectral response, but low ranges in red reflectance limit the sensitivity of this index over the dense canopy. Second, a basic assumption of the NDVI is that the spectral reflectance curve is that of a typical living plant, where reflectance in the NIR can be $\geq$ 70% higher than reflectance in the visible region of the light spectrum (Figures 1 and 2). However, the topical application of some pigmented products (e.g., turf colorants, pesticides with pigmented additives) has been shown to greatly influence the spectral response patterns in turfgrass, which impacts the interpretation of NDVI when NIR wavelengths between 730 and 850 nm are used. In these cases, it is recommended to use alternative indices such as the green-to-red ratio index (GRI) or photochemical reflectance index (PRI) that utilize regions of the light spectrum unaffected by the pigment but remain sensitive to plant status (McCall et al., 2021).

Other considerations include turfgrass cultural practices that may affect NDVI such as turfgrass species, mowing height, and sand topdressing, because these practices impact canopy geometry, shading, and surface features (Bremer et al., 2011a; Lee et al., 2011; An et al., 2015; Alvarez et al., 2016). Considering the impact of cultural practices on the response and interpretation of data, consistency in data collection, flight planning, and analysis can mitigate variability in spectral response associated with those cultural practices.

3 Critical mission planning

Important considerations must be made prior to initiating data collection protocols using sUAS in turfgrass. These considerations should clearly (i) identify the target of interest, (ii) specify resolution requirements to adequately assess the target of interest, (iii) determine the appropriate sensors to be used, (iv) identify an aircraft suitable for mounting the desired sensors, (v) determine appropriate flying altitudes, image overlapping settings, and travel speeds to achieve the desired spatial resolution, and (vi) identify the frequency at which data should be collected. Once these parameters are defined, planning and implementation of flights may proceed.

3.1 Defining the target of interest

It is critically important to accurately identify the target of interest as the first step in planning for data collection, as this greatly influences other parameters. For many situations, turfgrass response to various abiotic and biotic stresses will be the target of interest. Examples include monitoring turfgrass performance during abiotic stresses such as drought, heat, cold, salinity, herbicide application, or traffic as well as monitoring turfgrass performance during biotic stresses such as disease infection or insect feeding. However, the target of interest does not exclusively have to be turfgrass response. For certain missions, investigators may focus on quantifying disease severity or weed pressure, for example. In these situations, the targets of interest would be identifying specific disease symptoms or weed species present.

Consider a situation (scenario 1) where an investigator is interested in collecting data on small plot (0.9 m x 1.5 m) turfgrass research trials to monitor dollar spot (caused by *Clarireedia* spp.) disease activity. Alternatively, consider a second situation (scenario 2) where an investigator is interested in collecting data to identify large-scale drought stress patterns across a 40 ha golf course facility. The appropriate flight plans for these two situations will be extremely different from each other.

For scenario 1, there are at least two targets of interest that could be defined for the mission. The investigator could identify turfgrass performance as the target of interest and plan a mission to assess percent green cover (PGC) within a given area. However, the investigator could also identify dollar spot infection centers as the target of interest and plan a mission to quantify the number of infection centers within a given area. Both approaches are logical, and either could work for this scenario. Of greatest importance is that the investigator clearly defines the target of interest.

For scenario 2, there are also options available when identifying the target of interest. At this scale, the benefits of high-resolution imagery must be weighed against some logistical constraints. For instance, time to acquire data, number of batteries needed to complete the mission, and most importantly the size of the dataset to be processed (in gigabytes). Once the target resolution has been decided, imagery is most often used as a means to calculate PGC or measure relative differences in stress using common vegetation indices.

3.2 Critical resolution requirements

In the above scenarios, the resolution requirement for identifying dollar spot infection centers in small plot research trials will be much higher than that needed to identify large-scale drought stress patterns across a golf course facility. In turn, this will directly influence subsequent decisions for sensor type, aircraft selection, flight altitude, image overlapping, and travel speed, all of which will impact total data collection time. Moreover, higher resolution data will increase the total size of resulting datasets; thus, ground resolution thresholds should be identified to adequately reflect the needs of the mission. For example, spatial resolution requirements should be determined based on the size of the target of interest. If the target of interest (i.e., disease expression, localized dry spot, nutrient stress) is most noticeable at 4 cm in diameter, a spatial resolution of 1-2 cm^2 per pixel may be necessary to accurately capture targets due to image overlapping and distortion concerns (discussed further in sections 3.5 and 4.3).

3.3 Selection of appropriate sensors

There are various sUAS-mounted sensors available for monitoring turfgrass response, but there is often a single sensor that will be best suited for the task at hand. Many of the tools available at present are optical sensors that capture plant interactions with light. Examples include visible light sensors, spectral sensors, thermal sensors, and fluorescence sensors. There are important advantages and limitations to each of these and they have been thoroughly reviewed previously (Deery et al., 2014; Li et al., 2014; Fahlgren et al., 2015; Zhang and Zhang, 2018; Chandel et al., 2020; Sangha et al., 2020; Tmušić et al., 2020; Feng et al., 2021).

Sensor options can be divided into four primary categories: visible light, multispectral, hyperspectral, and thermal. Visible light sensors, also called true color or red, green, blue (RGB) sensors, measure light in three wide bands (i.e., red, green, and blue) and are typically used for high-resolution data acquisitions necessary for fine feature detection (e.g., weed identification and disease onset). At the time of this publication, true color sensors are the least costly and provide numerous opportunities unique to turfgrass systems because of the relative uniformity across targeted fields of interest. While there are only three bands to explore, the combinations of digital pixel values within these three bands allow for differentiating approximately 16 million unique colors (Yucky et al., 2021). Many emerging uses of artificial intelligence and machine learning for pest identification utilize only true color images.

Multispectral sensors measure light spectra in discrete bands that are often 20 – 100 nm in width, while hyperspectral sensors measure light spectra in much smaller (< 10 nm) increments that are usually continuous across the spectrum of measurement. For example, a hyperspectral sensor may record spectra in 2 nm increments from 450 nm to 1100 nm while a multispectral instrument will record spectra in five or more select regions and each region will be 10 or more nm wide. These “regions” of the light spectrum that are monitored are oftentimes referred to as “bands”. Hyperspectral sensors are designed to collect discrete measurements of reflected energy in hundreds of short bandwidths across the spectrum; bandwidths are typically much narrower than those of multispectral sensors. Hyperspectral data allow scientists to isolate discrete regions of the plant reflectance spectrum that are related to very specific plant attributes (e.g., carotenoids, anthocyanins, lignins, water stress, and disease). Hyperspectral sensors produce more data, which has advantages and disadvantages. Analyzing data with narrow spectral bandwidth may provide opportunities for detecting subtle changes that a multispectral sensor may miss but comes at a cost in both equipment expense and time required for data processing.

Thermal bands are increasingly available as well and allow the user to assess how well a plant canopy can dissipate heat. When transpiration rates are compromised, plants will emit long wave energy as a means to dissipate heat (i.e., sensible heat flux) (Hatfield et al., 2008). It is less efficient than transpiration, thus long wave emittance is positively correlated with plant stress (Bremer and Ham, 1999; Bremer et al., 2001; Sullivan et al., 2007; Peterson et al., 2017).

3.4 Selection of suitable aircraft

Unmanned aircraft systems are typically categorized as either fixed-wing or multicopter aircrafts. These platforms are quite different in terms of payload, run time, maneuverability, initial costs, and maintenance costs (Li et al., 2014). Fixed-wing aircrafts are regarded as having higher payloads, longer run times, and faster travel speeds, meaning they can accommodate more onboard sensors and other data recording instruments and they can cover more ground surface area in a given time, compared to multicopter aircrafts (Boon et al., 2017). However, operators must be conscious of potential image-blurring issues and ensure that onboard sensors will be compatible with the fast travel speeds of fixed-wing aircrafts. Many fixed-wing aircrafts also require large takeoff and landing areas and do not have the ability to hover in one location. Multicopter aircrafts have the capability to travel at slower speeds and maintain stable speeds at lower altitudes, often giving them an advantage for applications where high spatial resolution data are required (Thamm et al., 2015). However, multicopter aircrafts have lower payloads and shorter flight time capacities than fixed-wing aircrafts (Cai et al., 2014). Single rotor and fixed-wing hybrid vertical take-off and landing (VTOL) aircrafts are other options, though to date have been less used. Single-rotor helicopters are slower, with improved longevity and the capacity to carry heavier payloads but are also more expensive and potentially dangerous to operate. The fixed-wing hybrid has VTOL capacity and is an emerging option for improved flight endurance. Given the various differences in sUAS, much thought should be taken for the selection of the appropriate type of aircraft (Li et al., 2014).

3.5 Flight planning

Careful attention should be given to decisions concerning flight altitude, image overlapping, and travel speed. In general, higher flight altitudes will generate lower resolution data. Nonetheless, more ground surface area can be covered in a given time with higher altitudes. Thus, the tradeoff in data collection time and data resolution must be considered. This underscores the previous statement that it is essential to identify appropriate resolution thresholds for a given target of interest, as there is no added benefit to acquiring higher resolution data than is needed to assess the defined target of interest. Image overlapping is the amount of redundancy between data taken from adjacent viewpoints. In general, the higher the overlapping rate, the higher the final data resolution will be. In most agricultural applications, a minimum frame front and side-lap (i.e., image overlap in the forward and lateral directions) of 70 to 80% is required for accurate stitching of individual frames to generate a single composite image, known as an orthomosaic. Again, the target resolution must be kept in mind when deciding on an appropriate image overlapping setting. Travel speed is another variable that can impact total data collection time. However, travel speed constraints will generally be determined by the type of aircraft that is being used and the shutter speeds of the onboard sensor equipment. Nonetheless, a higher travel speed will enable faster data collection across a larger ground surface area in a given time.

3.6 Data collection frequency

This is the time interval between flights required to adequately monitor the identified target of interest. The proper collection frequency will largely depend on the dynamics of the target of interest. For example, if the target of interest changes rapidly, such as foliar disease progression or drought stress development, a weekly or daily collection frequency may be required. However, if the target of interest is more stable, such as genetic color, a monthly collection frequency may be adequate. Also keep in mind that certain targets, such as some patch diseases or weed inflorescence, may have a finite period for data collection. Careful planning before this critical window of opportunity will lead to fewer mistakes and wasted efforts due to insufficient data collection. These types of decisions will require input from expert personnel who understand the various targets of interest.

4 Data processing considerations

4.1 Unique characteristics of sUAS-acquired remote sensing data

Unlike satellite and aircraft imagery, sUAS acquire imagery as a steady stream of frames, or images, which are "stitched" together to produce a final image mosaic, as discussed previously (section 3.5). The resulting mosaic is a product of platform (aircraft) choice, sensor (payload), and flight planning as well as time of day and atmospheric conditions during data capture. Time of day and atmospheric conditions are critical because to date, sUAS-mounted sensors are typically passive (i.e., do not have their own light source, as opposed to active sensors) and thus, are impacted by factors such as sun angle and cloud cover (Campbell, 1996).

4.2 Calibration

Although platform, sensor choice, and flight planning are critical first steps, image pre-processing and calibration significantly impact the digital integrity of the image product. Uncalibrated images represent an "at-sensor" measurement of reflectance or more simply the amount of reflected light from the vegetation surface that was received by the sensor. At-sensor, or uncalibrated measurements are subject to conditions during the instant of data capture such as sun angle (time of day), atmospheric conditions, surface conditions, and canopy geometry. Calibration techniques are designed to adjust uncalibrated values to "at-target" values by correcting the at-sensor measurement for atmospheric conditions during the time of capture. When successful, calibrated measurements should provide a measurement of plant response that may be compared from flight-to-flight (time-series measurements).

Image calibration is typically accomplished using a combination of camera-specific settings or metadata, ground calibration targets, and paired measurements of downwelling (irradiant) and upwelling (reflected) energy. Downwelling light measurements are typically collected during flight by an upward-facing sensor on the aircraft, while calibration panel measurements are often collected manually pre- and post-flight with the onboard down-facing sensor. Although commonly used, reference panels can considerably impact the calibrated reflectance in both positive and negative ways. Considering that calibration panels are typically used pre- and post-flight, two new sources of error arise if calibration data are not acquired carefully: 1) human error during panel capture, and 2) potential variability in conditions during flight that is not representative of conditions during the time of panel capture. Examples that could negatively affect the representativeness of panel calibrations include (i) partly cloudy conditions and (ii) extended flight times when the angle of incident energy and/or cloud cover may vary significantly. For these reasons, the effective use of calibration panels and incorporation of downwelling irradiance at low altitudes is still the subject of ongoing research (Assmann et al., 2018; Delvapour et. al, 2021).

4.3 Image processing packages: Research grade versus edge-of-field

Image processing can be placed into two categories: pre-processing and post-processing. During the pre-processing phase, individual frames are mosaicked (stitched) into a single image composite (orthomosaic). It is during this phase that camera-specific settings, calibration data, and even the spatial resolution of the final image product are applied. The scope of the flight mission and ultimate use of image products will impact image processing decisions. Considerations include overall area, need for real-time assessments, target size and spatial resolution requirements, and research-grade versus field-grade requirements. For example, an edge-of-field solution, which is intended to provide near-real-time results, may be appropriate for a field-scale mission (> 10 ha for example). Edge-of-field solutions are appropriate when image turn-around time needs to be fast and spatial resolution requirements are > 10 cm^2 per pixel, such as with rapid assessments of drought stress. In this example, the number of key points selected during the stitching process may be greatly reduced and filters may be used to smooth the final image product.

Alternatively, a research grade approach may be taken when the target area is smaller, spatial resolution requirements are higher (sub-centimeter to < 10 cm^2 per pixel) and more rigorous image processing parameters are required to retain the digital integrity of the dataset (e.g., calibration, increased number of key points, reduced filtering/smoothing assumptions, bidirectional reflectance corrections, band to band alignment, geo-registration) (van der Merwe et al., 2020). Ultimately, a research-grade product increases the processing time required and can generate a much larger dataset given its high spatial resolution requirements.

As a real-world example of how spatial resolution can impact a data product, consider a 38 ha location flown by one of the coauthors. When the as-flown image spatial resolution was 3 cm^2 per pixel, the generated image file size was 2.5 gigabytes. However, when the resolution was decreased to 6 and 10 cm^2 per pixel, the generated image file sizes were only 615 and 222 megabytes, respectively. Therefore, as spatial resolution requirements of the target of interest increase, the raw file sizes used to generate these images increase by orders of magnitude.

Software service providers often estimate costs based on these parameters as well. Taking all aspects of a flight mission into consideration (elevation, speed, overlap, spatial resolution, number of bands, and temporal resolution) will define the amount of data in gigapixels that are acquired, prior to any post-processing costs (time and expense). Gigapixels are determined based on the number of images multiplied by the image pixel width and height, number of bands, and number of flights. Since most cameras have a fixed image pixel count, the number of frames per mission increases/decreases with altitude, speed, and overlap. Although cloud-based image processing solutions are prevalent today, moving large amounts of data via the cloud is still inefficient.

5 Examples of sUAS applications in turfgrass

5.1 Drought assessment and detection in turfgrass

Few studies have investigated drought stress in turfgrass using sUAS. Those few studies have demonstrated that drought stress was successfully detected using spectral or thermal sensors mounted on sUAS (Table 1). In a three year study involving deficit-irrigated creeping bentgrass (*Agrostis stolonifera* L.) mowed at golf course fairway-height (15.9 mm), drought stress was detected with six of eight spectral VIs evaluated, which were derived from broadband reflectance in the NIR, green, and blue (e.g., Blue NDVI, NDVI Enhanced2, NIR BlueRatio, GreenBlue; Table 1) (Hong et al., 2019b). Correlations of those six VIs with visual turf quality ratings (TQ) and PGC from ground-based measurements with a digital camera, which were indicators of canopy drought stress, ranged from r = 0.68 to 0.87 (TQ) and r = 0.71 to 0.92 (PGC). In the same study, the NIR broadband also detected drought stress (TQ, r = 0.65 to 0.75; PGC, r = 0.68 to 0.84). Interestingly, early drought stress was detected with VIs before decreases in TQ and PGC (due to drought-induced leaf firing) were observed. Specifically, indices that detected early drought stress included Blue NDVI, NDVI Enhanced2, and NIR Blueratio in treatments irrigated at 15 and 30% reference evapotranspiration (ET_o) replacement ($P < 0.05$). However, the most consistently sensitive parameters of sUAS were the GreenBlue VI and the NIR broadband, which detected drought stress >5 d before decreases in TQ over the three-year study (Figure 3). Thus, both reflectance from an individual broadband (NIR) and VIs derived from multiple broadbands demonstrated strong capabilities for detecting drought stress in turfgrass.

Table 1. Spectral, red-green-blue (RGB), and thermal measurements and vegetation indices that detected drought stress from small unmanned aircraft systems (sUAS) and ground-based platforms in turfgrass field studies.

Sensor	Index	Description	Relationship with drought stress variables	References
		sUAS-based		
Spectral	NDVI	Normalized difference vegetation index: (NIR−red)/(NIR+red)	Leaf relative water content, r = 0.96; Soil moisture r = 0.82 to 0.86	(Caturegli et al., 2020)
			Turf quality (TQ), R^2 = 0.13 to 0.68; Percent green cover (PGC), R^2 = 0.73 to 0.88; (two species).	(Zhang et al., 2019b)
	Blue NDVI	(NIR−blue)/(NIR+blue)	TQ, r = 0.77 to 0.87; PGC, r = 0.83 to 0.92.	(Hong et al., 2019b)
	NDVI Enhanced2	(NIR+green−blue)/ (NIR+green+blue)	TQ, r = 0.76 to 0.87; PGC, r = 0.82 to 0.92.	(Hong et al., 2019b)
	NIR Blueratio	NIR−blue	TQ, r = 0.77 to 0.86; PGC, r = 0.83 to 0.90.	(Hong et al., 2019b)
	WBI	Water band index: R_{900} / R_{970}	Soil moisture, r = 0.87 to 0.89; Leaf relative water content, r = 0.98.	(Caturegli et al., 2020)
	NDRE	Normalized difference red edge: (NIR−red edge)/(NIR+red edge)	Spearman's rank correlation: TQ, r = 0.60; PGC, r = 0.68; (2 species).	(Zhang et al., 2019b)
RGB	GreenBlue	(green−blue)/(green+blue)	TQ, r = 0.68 to 0.86; PGC, r = 0.71 to 0.91.	(Hong et al., 2019b)
	VARI	Visible atmospherically resistant index: (green−red)/(green+ red−blue)	TQ, R^2 = 0.05 to 0.63; PGC, R^2 = 0.69 to 0.89; (2 species).	(Zhang et al., 2019b)

Thermal	Tc	Canopy temperature	TQ, r = -0.77; PGC, r = -0.78.	(Hong et al., 2019a)
	Tc-Ta	Canopy and air temperature difference	TQ, r = -0.60; PGC, r = -0.58.	(Hong et al., 2019a)
		Ground-based		
Spectral	NDVI	Normalized difference vegetation index: (NIR−red)/(NIR+red)	TQ, r = 0.87 to 0.90; PGC, r = 0.92 to 0.95.	(Hong et al., 2019b)
			Soil volumetric moisture at 0% ET_o treatment, r = 0.54	(Badzmierowski et al., 2019)
	SAVI	Soil adjusted vegetation index: $(1.0 + L)(R_{830} - R_{660})/(R_{830} + R_{660} + L)$; usually L=0.5	Non-linear relationship with ET_o treatments (Lower SAVI at bottom ET_o treatments)	(Taghvaeian et al., 2013)
RGB	PRI	Photochemical Reflectance Index: $(R_{531} - R_{570}) / (R_{531} + R_{570})$	Color, $R^2 = 0.58$; Tissue moisture content, $R^2 = 0.73$.	(Baghzouz et al., 2007)
	GRI	Green-to-red ratio index: R_{550} / R_{670}	Soil volumetric moisture at 0% ET_o treatment, r = 0.54	(Badzmierowski et al., 2019)
Thermal	Tc-Ta	Canopy and air temperature difference	Vapor pressure deficit of non-water-stressed turf, r = 0.64 to 0.88 (2 species)	(Haghverdi et al., 2021)
	CWSI	Crop water stress index: $[(Tc\text{-}Ta)_{measured} - (Tc\text{-}Ta)_{lower}]/[(Tc\text{-}Ta)_{upper} - (Tc\text{-}Ta)_{lower}]$	Non-linear relationship with ET_o treatments (Lower CWSI at bottom ET_o treatments)	(Taghvaeian et al., 2013)
			Seasonal CWSI average: A non-linear relationship with color; Threshold for seasonally acceptable color= 0.1	(Emekli et al., 2007)

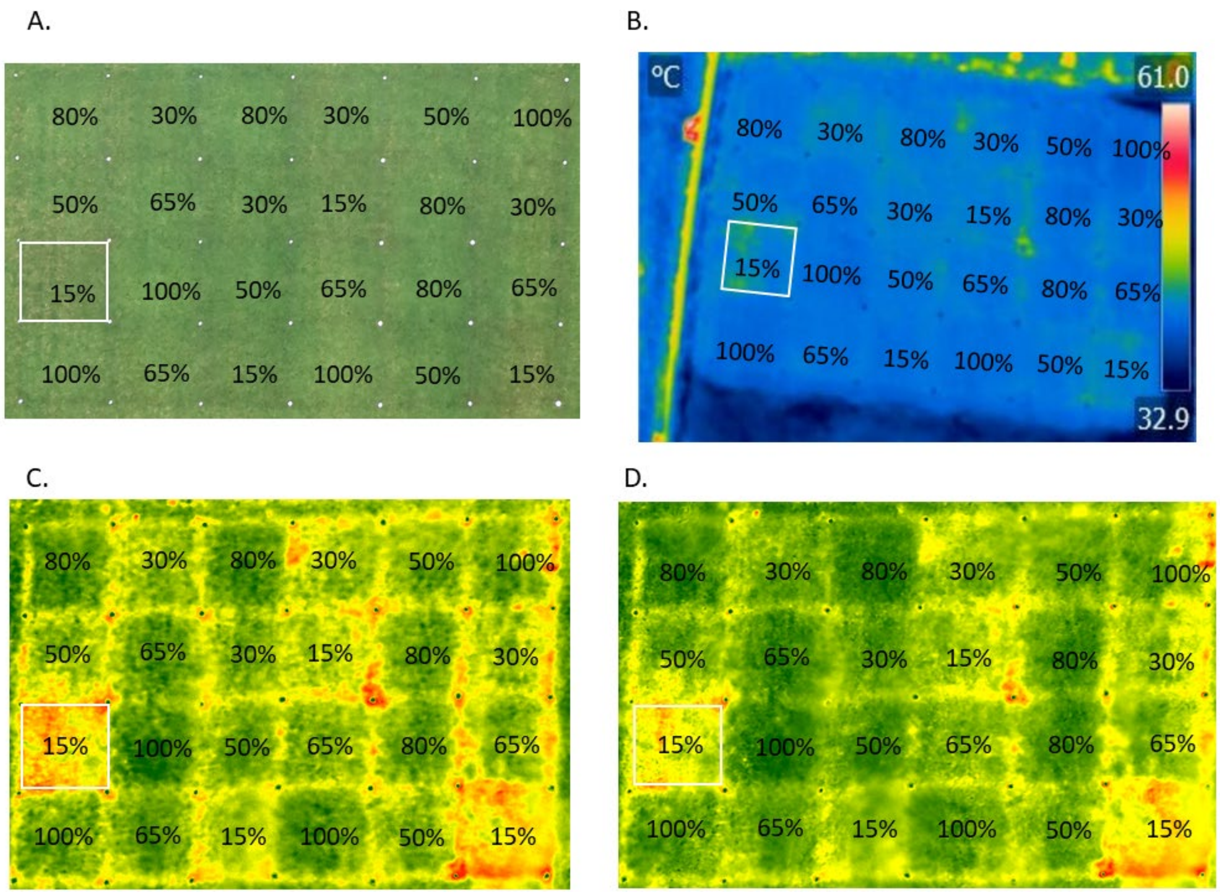

Figure 3. A red-green-blue (RGB) image (A), thermal image (B), GreenBlue VI orthomosaic (C), and NIR reflectance orthomosaic (D) on June 15, 2017 of a sUAS study. Data were collected six days after deficit-irrigation treatments (15 to 100% ET_o) began (Hong et al., 2019a, 2019b).

As discussed earlier (section 3.3), VIs calculated from wavebands strictly in the visible region of the spectrum may be produced from sUAS-based RBG images (i.e., without wavebands in the NIR or higher) and used to evaluate drought stress in turfgrass (Caturegli et al., 2019; Hong et al., 2019b; Zhang et al., 2019b). For example, the GreenBlue VI mentioned above (in the 3 yr sUAS study in deficit-irrigated creeping bentgrass plots) utilized green and blue wavebands in the visible region of the spectrum and was highly sensitive to drought stress in turfgrass, and it consistently detected drought stress earlier than seven other VIs (Table 1; Figure 3) (Hong et al., 2019b). The visible atmospherically resistant index (VARI; Table 1), which uses green and red wavebands in the visible spectrum and was developed to reduce atmospheric effects (Gitelson et al., 2002), was strongly correlated with PGC of turfgrass under drought stress in a sUAS study (Zhang et al., 2019b). The dark green color index (DGCI) derived from sUAS RGB images was highly correlated with sUAS measurements of NDVI ($r = 0.85$ to 0.96; under different N fertilization regimes), which implies DGCI might be used in lieu of NDVI to detect drought-induced leaf firing when spectral sensors that measure NIR reflectance are not available (Caturegli et al., 2019); strong relationships between NDVI and PGC in turfgrass have been reported by others using sUAS-based measurements (Bach et al., 2022a) and ground-based measurements (Bell et al., 2002; Bremer et al., 2011b).

Canopy temperature is another powerful indicator of early drought stress, including when measured from sUAS. For example, only six days after initiation of deficit irrigation treatments in small plots of creeping bentgrass, early drought stress was detected from a single image taken with a sUAS-mounted thermal camera (Hong et al., 2019a). Specifically, higher canopy temperature was detected in deficit-irrigated plots (15 and 30% ET_o; $P < 0.05$), before decreases in TQ and PGC were observed (Figure 3). For larger areas such as golf courses, numerous thermal images would be required because of the limited footprint area per image and viewing angle effects among images, and thermal orthomosaics would need to be generated (van der Merwe et al., 2017, 2020). To evaluate changes over time, the timing of canopy temperature acquisition should be consistent and documented (e.g., data collected at approximately the same hour on each measurement day) (Mauri, et al., 2021) and atmospheric conditions should be comparable among days (e.g., cloud-free) (Hong et al., 2019a). More research is needed to develop standard sampling and processing protocols for measuring canopy temperature with thermal cameras mounted on sUAS (Chandel et al., 2020; Sangha et al., 2020; Tmušić et al., 2020). There are tradeoffs regarding camera resolutions, sensitivities to viewing angle effects, and appropriate flying heights when selecting thermal sensors with different lenses, that are beyond the scope of this discussion (Sangha et al., 2020).

5.1.1 Relationships between aerial and ground-based measurements

Most remote sensing research in turfgrass has been ground-based in regard to using spectral reflectance to detect drought stress. However, recent sUAS studies have indicated moderate to strong correlations between ground- and sUAS-based measurements of spectral reflectance in turfgrass. Correlations between ground- and sUAS-based NDVI ranged from r=0.63 to 0.97 in a number of turfgrass studies (Caturegli et al., 2016; Hong et al., 2019b; Zhang et al., 2019b; Friell and Straw, 2021; Bach et al., 2022a, 2022b). Hong et al. (2019b) also reported strong correlations (r=0.69 to 0.87) between sUAS-based broadband NIR (about 680-780 nm) and ground-based narrowband NIR (around 780 nm) in drought-stressed turfgrass. Therefore, ground-based measurements of drought-sensitive VIs, as well as individual wavebands would likely be applicable to their counterparts measured with sUAS-mounted sensors, although more research is required.

An example of a VI that is highly sensitive to drought but has only been evaluated using ground-based measurements in turfgrass is the PRI, which utilizes green and blue wavebands (Table 1). The PRI may have advantages over NDVI in detecting minor drought stress because of certain phytochemical changes that may occur before changes in biomass and color become evident (Zarco-Tejada et al., 2012; Gago et al., 2015; Barbedo, 2019). For example, stomatal conductance and water potential were more strongly correlated with PRI than with NDVI in a sUAS study conducted over an orange tree canopy (Zarco-Tejada et al., 2012). In turfgrass, initial results are promising from ground-based PRI applications in monitoring drought stress (Baghzouz et al., 2007; Table 1). Additional VIs obtained from ground-based RGB images have also been shown to be sensitive indicators of drought stress (Marín et al., 2020). The soil adjusted VI (SAVI; Table 1), which uses the NIR broadband in its calculation, statistically detected drought stress in ground-based measurements of low vs. high irrigation treatments (Taghvaeian et al., 2013). In the future, drought-sensitive VIs that have only been evaluated in ground-based turfgrass studies need to be tested in sUAS research (Badzmierowski et al., 2019; see additional VIs summarized by Baghzouz et al., 2007).

Other ground-based research has identified specific narrowbands and broadbands in the visible to NIR spectrum that were indicators of drought stress in several turfgrass species and cultivars under field settings. For example, narrowbands (2-5 nm) that indicated drought stress ranged from 660 to 672 nm in several popular C3 turfgrasses, and from 555 to 870 nm in C4 turfgrasses (Table 2). The water band index (WBI), centered around 970 nm and 900 nm, has proven effective for estimating drought stress in creeping bentgrass and hybrid bermudagrass [*Cynodon dactylon* (L.) Pers × *Cynodon transvaalensis* Burtt Davy], as well as in other crops (Peñuelas et al., 1993; McCall et al., 2017; Caturegli et al., 2020; Roberson et al., 2021). Also, individual broadbands centered at 830 nm (NIR) and 1650 nm (short-wave infrared, SWIR) responded to drought stress, to a lesser extent than visible bands, in several turfgrass species (Taghvaeian et al., 2013). Field studies are warranted to use sUAS to leverage information obtained from ground-based remote sensing research regarding drought-sensitive wavebands that predict drought stress across different turfgrass species and cultivars.

Table 2. Narrow spectral wavebands with high correlations to drought stress in C3 (top) and C4 (bottom) turfgrasses from ground-based field studies.

Species	Wavelength (nm)	Linear relationships with variables	References
		C3 Turfgrasses	
Tall fescue (*Festuca arundinacea* Schreb.)	671	Turf quality (TQ): r = -0.39 to -0.60; Leaf firing: r = 0.44 to 0.67 (3 cultivars)	(Jiang and Carrow, 2005)
Kentucky bluegrass (*Poa pratensis* L.)	672	Leaf water content: R^2 = 0.71 to 0.96	(Suplick-Ploense et al., 2011)
Hybrid bluegrass (*Poa pratensis* L. x *Poa arachnifera* Torr.)	664, 668	Leaf water content: R^2 = 0.78, 0.80	(Suplick-Ploense et al., 2011)
Perennial ryegrass (*Lolium perenne* L.)	660, 664	Leaf water content: R^2 = 0.88, 0.84	(Suplick-Ploense et al., 2011)
Annual ryegrass (*Lolium multiflorum* Lam.)	693	Tissue moisture: R^2 = 0.71	(Baghzouz et al., 2007)
		C4 Turfgrasses	
Zoysiagrass (*Zoysia japonica* Steud.)	687	TQ: r = -0.49; Leaf firing: r = 0.54	(Jiang and Carrow, 2005)
St. Augustinegrass [*Stenotaphrum secundatum* (Walt.) Kuntze]	687	TQ: r = -0.23	(Jiang and Carrow, 2005)
	693	Leaf firing: r = 0.23	
Hybrid bermudagrasses [*Cynodon dactylon* (L.) Pers. × *C. transvaalensis* Burtt Davy]	555	Tissue moisture, color, soil matric potential, leaf xylem water potential: R^2 = 0.66 (multiple regression predicting R_{555})	(Baghzouz et al., 2007)
	667-693	TQ: r = -0.15 to -0.48; Leaf firing, r = 0.32 to 0.62; (4 cultivars)	(Jiang and Carrow, 2005)
Seashore paspalum (*Paspalum vaginatum* Swartz)	750, 775, 870	TQ, r = 0.15 to 0.48; Leaf firing, r = -0.40 to -0.47 (3 cultivars)	(Jiang and Carrow, 2005)

Three to five broadbands, mostly from the absorption regions of chlorophyll (660-700 nm) and water (810-1480 nm), were used to develop optimum regression models for TQ (R^2 = 0.33 to 0.78) and leaf firing (R^2 = 0.16 to 0.83) under drought stress in 11 cultivars of five turfgrass species (Jiang and Carrow, 2007). Besides using multiple regressions of several bands (Baghzouz et al., 2006, 2007; Jiang and Carrow, 2007), the utilization of ground-based narrowbands across the entire visible and NIR spectrum and their derivatives has also shown advantages over VIs in the early detection of drought stress in pasture grass via the use of machine learning algorithms (Dao et al., 2021). Given the availability of sUAS-mounted hyperspectral sensors, selecting wavebands across wide regions, or taking advantage of the full spectrum from visible to mid-infrared wavebands instead of merely a few wavebands for VIs may provide a more robust solution for detecting drought stress, and warrants further research in turfgrass field studies.

5.2 Strategic cultivar selection in turfgrass breeding programs

Turfgrass breeders are limited in their field phenotyping capability due to its high requirement of time and labor. Being able to collect comprehensive data during the early stages of selection and then later in advanced trials would benefit cultivar selection and improvement in turfgrass breeding programs. As technology advances, the use of sUAS in high throughput phenotyping has increased rapidly in the past five years (Tattaris et al., 2016; Holman et al., 2016; Yang et al., 2017; Han et al., 2019; Li et al., 2020). Unlike many other agronomic crops, yield is not a breeding goal for turfgrass. Superior turfgrass lines are selected based on their phenotype, commonly known as phenotypic selection (Islam et al., 2014), which is ideal for evaluating with sUAS-based imagery. Zhang et al. (2019b) assessed the use of sUAS-based RGB and multispectral imageries on variety trials of two warm-season turfgrass species – bermudagrass (*Cynodon* spp.) and zoysiagrass (*Zoysia* spp.), using a low-cost sUAS platform. In the study, ground truth measurements were compared with sUAS-based measurements, and out of the top ten entries identified using ground measurements, 92% (bermudagrass) and 80% (zoysiagrass) overlapped with those using sUAS-based imagery. A collaborative project was initiated in late 2019 to equip turfgrass breeding programs in the southeastern U.S. with sUAS-based high-throughput phenotyping tools (Zhang et al., 2019a). This ongoing project aims to enhance the phenotyping capability of turfgrass breeders and further the application of sUAS in turfgrass breeding programs.

Despite the subjectivity of visual TQ ratings (Horst et al., 1984), it has been the primary evaluation method for many years (Karcher and Richardson, 2013). Digital image analysis (DIA) was implemented as a research tool starting around the 1980s and turfgrass scientists adapted it into routine data collection with standardization in relevant equipment and image processing (Richardson et al., 2001). Equipment usually includes a “light box”, which is a metal box with light bulbs and wheels to be pushed across test plots. A camera is inserted on the top of the metal box to take pictures. Various turfgrass parameters are derived from DIA such as PGC, turf color, turfgrass establishment, drought stress, divot analysis, wear tolerance, and disease analysis (Patton et al., 2007; Steinke et al., 2010; Trappe et al., 2011a, 2011b; Karcher and Richardson, 2013; Zhang et al., 2018; Bach et al., 2022a, 2022b). This method has worked well in turfgrass research except that it remains time consuming for turfgrass breeders to collect pictures on thousands of field plots in a timely manner. Based on previous validation work, a sUAS can collect images covering thousands of small plots (0.9 x 1.5 m) in a few minutes versus days of collecting data with a light box, during which time PGC could be changing among plots.

The general workflow of sUAS was described earlier, but briefly includes image acquisition using sUAS, image processing and orthomosaic generation, and plot-level data extraction. In addition, consideration of data analytics is needed because larger amounts of data are generated from sUAS than with traditional phenotyping methods. Image acquisition involves sUAS and sensor selections as well as best practices in flight operations (described earlier). Image processing is carried out by commercial software such as Pix4DMapper (Pix4D SA, Lausanne, Switzerland) and Agisoft metashape (Agisoft LLC, St.Petersburg, Russia) to generate orthomosaics. Plot-level data extraction can be done using ArcMap or QGIS (Wilber et al., 2021). But for large data extraction, faster workflows can be built in different programming languages such as R (R Core Team, 2021) and python (Van Rossum and Drake, 2011). Commercial software such as Phenix™ (Progeny Drone Inc., Lafayette, IN, USA) and TurfScout & AgSpect (TurfScout, LLC. Greensboro, NC, USA) is available for combining image processing and data extraction together.

Similar to the aforementioned DIA using a light box, sUAS-based image analysis can extract traits such as turfgrass cover in both dormant and green vegetation and plot-based average vegetation and color indices. There are different methods to obtain PGC from sUAS-based imagery. For multispectral imagery, PGC can be calculated by thresholding NDVI. For RGB imagery, two different methods can be used: one is thresholding color index from RGB imagery, and the other is converting RGB imagery to Hue/Saturation/Brightness and using threshold values for Hue and Saturation to extract green pixels. Wang et al. (2022) evaluated a comprehensive combination of approaches for estimating turfgrass PGC using sUAS imagery. These approaches, varying in levels of complexity, were based on VIs, supervised and unsupervised machine learning classification, and image processing methods. They found that both RGB image-based PGC estimation methods, including the Hue-Saturation-Value method and the support vector machine agreed with ground-measurements of PGC (R^2 = 0.86-0.96).

Turfgrass cultivar field trials can be monitored monthly for these traits with or without biotic and abiotic stress. Secondary traits such as rates of turfgrass establishment can be derived from repetitive measurements of turfgrass cover during establishment (Figure 4). Each breeding program may vary in its process of compiling the information and making selections. For instance, one widely used mechanism is to rank the genotypes based on the number of times a given genotype enters the top statistical group over multiple traits of interest or/and multiple dates; this is known as the turf performance index (Wherley et al., 2011; Zhang et al., 2019b). As large amounts of comprehensive data are being collected using high-throughput phenotyping, more sophisticated algorithms for genotypic ranking or/and for identifying stress tolerant genotypes is needed.

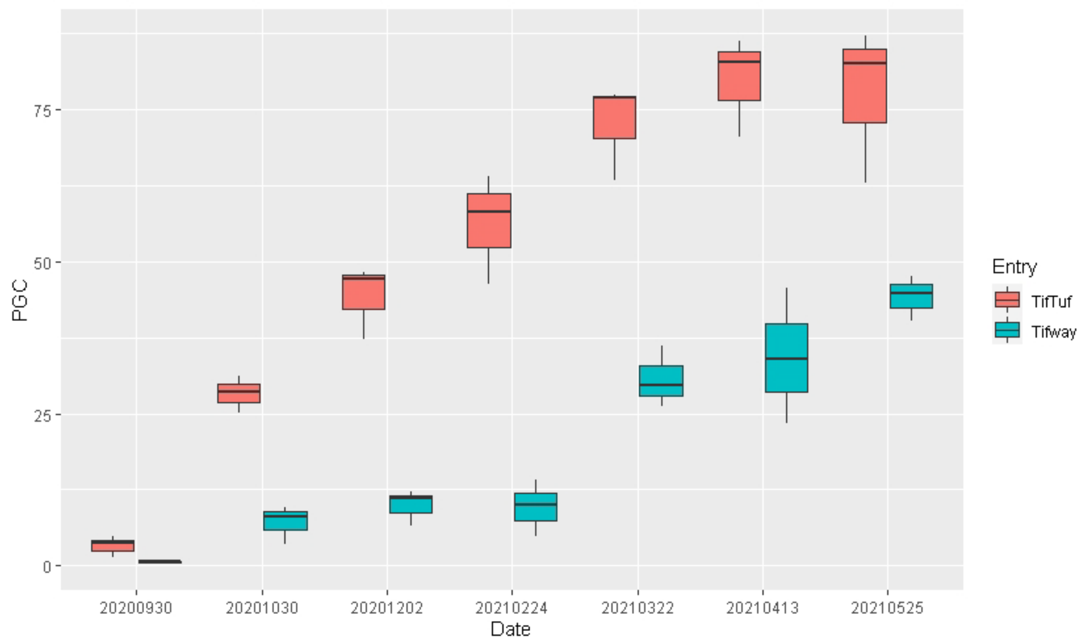

Figure 4. Boxplots of percent green cover (PGC, %) of two hybrid bermudagrass cultivars ('TifTuf' and 'Tifway') during establishment in Tifton, GA, USA.

One of the challenges in analyzing sUAS-based imagery for field phenotyping in turfgrass variety trials is weed contamination. Weeds can be problematic in the early stages of breeding selection (for instance, single plant space nursey) when management practices are less proactive compared to advanced trials. Supervised classification can be incorporated to exclude weeds in the workflow (Rockstad et al., 2020), which slows down the process due to the need for human input. In the future, it will likely be possible to implement machine learning models to mask weeds, but that would require a large number of labelled images to be collected in order to train a model.

5.3 Predicting/managing turfgrass pests

Much of this chapter has provided a strong overview of the factors to consider when using sUAS and associated aerial imagery from a variety of sensors across turfgrass systems. The use of these tools provides a unique opportunity for monitoring and managing pest outbreaks across large surfaces that have been previously impractical because of time constraints and overlooked because of not being able to scout all areas effectively. While the use of sUAS to monitor and predict pest outbreaks is still in its infancy, there are a few examples that show promise as a shift towards precision turfgrass management.

5.3.1 Spatial distribution of pests

Most pest outbreaks are aggregated or occur in clusters, rather than being uniformly distributed across larger surfaces (Campbell and Noel, 1985). This is particularly true on maintained turfgrasses, though documentation through peer-reviewed research is limited. A better understanding of the spatial variability and distribution of pest outbreaks provides the opportunity for targeted pesticide applications, providing both economic and environmental benefits.

Henry et al. (2009) concluded that two common paspalum species, dallisgrass (*Paspalum dilatatum* Poir.) and bahiagrass (*Paspalum notatum* Flügge), are not uniformly distributed across bermudagrass golf course fairways or roughs. Rather, they tended to cluster in areas with underlying issues, such as compacted soils. The authors reported that bahiagrass was impacted by mowing height, as it was more commonly found in roughs than in fairways, whereas dallisgrass grew in both shorter (fairway) and taller (rough) heights-of-cut. The understanding of underlying edaphic and environmental factors that drive paspalum outbreaks provides a unique opportunity for targeted cultural management strategies to alleviate these conditions.

Annual bluegrass weevil (ABW) is an economically important pest in the northeastern United States that causes damage in a predictable pattern. Damage from ABWs typically first appear closest to tree-lines and other out-of-play areas where the adults overwinter (Diaz and Peck, 2007). Similarly, another economically important turfgrass insect pest, the hunting billbug (*Sphenophorus venatus vestitus* Chittenden), was shown to also have an aggregate (clustered) distribution across sod farms in Georgia, USA (Gireesh et al. 2021). Spurlock (2009) reported that large patch, caused by *Rhizoctonia solani* (Kühn) re-occurred in the same location of golf courses from year-to-year. This reoccurrence suggests an opportunity for strategic fungicide applications through disease incidence mapping.

Horvath et al. (2007) showed a strong and stable spatial aggregation of dollar spot on creeping bentgrass and annual bluegrass (*Poa annua* L.) across seasons, even as overall disease pressure continued to increase. While the geospatial location of dollar spot aggregates changed from year to year, the clustering relationship remained the same across seasons. This suggests that historical disease incidence maps may not be useful for site-specific management of dollar spot but aerial maps generated within season may provide valuable monitoring.

Most of the research to date that defines the spatial distribution of pests has been collected from intensive, time-consuming field sampling. While ground validation is critical for any confidence in pest estimations, much of the information could be collected rapidly and remotely using sUAS.

5.3.2 Pest mapping with aerial analysis

The most extensive use of sUAS to map a turfgrass pest for monitoring and management has been for assessing spring dead spot (caused by *Ophiosphaerella* spp.) of bermudagrass (Booth et al., 2021, Henderson, 2021). Booth et al. (2021) reported that spring dead spot developed in aggregates across golf course fairways in Virginia, USA. The authors demonstrated that spring dead spot frequently occurs in the same patches year after year, despite full bermudagrass recovery during the growing season. This understanding of the spatial and temporal dynamics of spring dead spot provided an opportunity for targeted fungicide applications. The authors reported using spring dead spot incidence maps to treat the disease site-specifically using a high spatial resolution global positioning system (GPS) sprayer without compromising efficacy. The result led to a decrease of 51% and 65% in fungicide use for the first and second years of the study, respectively.

The successful reduction of fungicides inputs using sUAS and targeted applications described by Booth et al. (2021) was not without challenges. Intensive manual selection of all spring dead spot within aerial imagery was not feasible for practical implementation by turfgrass professionals. Subsequent research provided a framework for automated detection without the need for manual selection or high-output computing (Henderson, 2021). The author also reported a detection accuracy with a 1 m buffer ranging from 53% to 93% compared to hand-validated pest maps. The author reported the diseased area with buffers covered between 4% and 21% of the fairways tested, providing the opportunity for substantial fungicides savings even greater than those reported by Booth et al. (2021). Follow-up research using spring dead spot mapping for targeted fungicide applications is ongoing.

The use of aerial pest mapping via sUAS provides a unique perspective on understanding the spatial and temporal dynamics of disease outbreaks or pest infestations. The disease incidence maps described above were used to help understand the underlying factors that drive spring dead spot epidemics. Hutchens et al. (2021) used the methods described by Henderson (2021) to compare zones of high, moderate, and low disease intensity. Results from this study suggested that the most influential factors to disease development included thatch accumulation and soil moisture, along with several key macro- and micronutrients. New research addressing the factors that drive dollar spot epidemics using the described strategies is ongoing (Henderson and McCall, 2021). Similar strategies using sUAS may be applied to numerous other diseases, weeds, and insect infestations to better understand their spread across turfgrass systems.

5.3.3 Remote pest detection using remote sensing and/or aerial imagery

The previous case studies have relied primarily on true-color imagery, using only red, green, and blue bands. However, there are many opportunities for detecting diseases and other pests using wavelengths outside of the visible light spectrum. As has previously been discussed in this chapter, the spectral properties of both uniform, healthy turfgrass stands and those physiologically altered from various stressors can be used for rapid assessments. However, there are few documented reports in the literature where light outside of the visible spectrum has been used to detect either pathogen activity or subsequent damage to turfgrass canopies. Green et al. (1998) reported a significant correlation between Rhizoctonia blight (aka brown patch) and several visible or NIR wavelengths, with 810 nm being the most closely related. However, the authors also pointed out that there were numerous extraneous factors that contributed to the decline in canopy reflectance beyond simply disease degradation. Henderson (2021) reported that thermal image analysis could be a useful tool to detect brown patch in tall fescue and creeping bentgrass, and could detect changes in pathogen load during pre-symptomatic pathogen infection and colonization.

5.3.4 Challenges with developing pest incidence maps

Developing any type of pest incidence map is merely a prediction of where the pests are located and will likely never be a perfect proxy for manual scouting. As with any type of modeling, the prediction is only as strong as the information provided when developing the model. Some challenges that may limit the accuracy of pest maps include the uniqueness of spectral properties of both the targeted pest and the intended turfgrass, the spectral or image resolution, the spatial resolution of both the aerial imagery and the ground validation dataset, and perhaps most importantly, the accuracy of proper ground validation of pests. Many pests or associated turfgrass damage may look very similar, particularly from dozens of meters above the surface. Predicted pest distributions from above will be rendered useless without proper and accurate verification from trained experts on the ground.

Another challenge with developing pest incidence maps for targeted management is that some expertise outside of the traditional fields of agronomy, plant pathology, entomology, and weed science are needed. This chapter includes excellent information on understanding spectral properties of plant canopies, mission planning, and data processing. A basic understanding of these core subjects is critical for proper adoption of remote pest mapping. Bock et al. (2010) discusses benefits, drawbacks, and opportunities of using hyperspectral image analysis, among other things for plant disease detection. Wei et al. (2021) provides an additional overview of pathogen/disease detection of peanuts and other important agronomic crops with remote sensors. Many of the principles discussed apply to turfgrass pest detection. Additionally, a basic understanding of computer science will allow for a smooth transition into automated pest mapping. Useful strategies to automate pest mapping include simple computer coding to more complex types of image classification, simple machine learning, and more complex deep learning. Some of these strategies are discussed in a review by Henderson (2021). Researchers have used a convolutional neural network to successfully identify and map various broadleaf and grassy weeds, spurges, and sedges in bermudagrass (*Cynodon dactylon* L.) sod fields (Zhang et al., 2021). Improvements in sUAS technology and sensor development, along with decreasing costs of equipment and increased computer processing outputs, provide a plethora of new opportunities to monitor, manage, predict, and better understand the behavior of various turfgrass pests.

6 Conclusions and future trends

The use of sUAS in turfgrass research and applied turfgrass management is emerging and offers many novel possibilities and unique challenges. Although remote sensing imagery acquired with sUAS has been the primary focus of this chapter, it is only part of the digital landscape. One promising strategy is to integrate sUAS remote sensing measurements with other data stream sources such as weather, soil moisture, as-applied fertilizer and pesticide maps, topography and basic soil descriptions, labor, and product inventory to enhance turfgrass management (Taghvaeian et al., 2013; Aboutalebi et al., 2019; Chávez et al., 2020; Chandel et al., 2021).

One example could include monitoring of drought stress by combining sUAS spectral reflectance or thermal measurements of the turf canopy with other critical data obtained from ground sensors or weather stations (e.g., soil moisture, forecasted reference ET_o). This information could be used to prevent drought stress while conserving water by improving irrigation recommendations, which could be further leveraged by using variable rate irrigation technology (Straw et al., 2019; Chávez et al., 2020; Dyer, 2022).

As we are able to acquire and create more data, “big data” management becomes increasingly important. The successful measurement, collection, and analysis of big datasets could promote a greater understanding of how and why a plant responds in a given way and allow us to better model and even predict expected outcomes. Such efforts will likely require algorithm development and cloud computing services, possibly by using artificial intelligence through machine learning neural networks, to efficiently process large data streams (Zhang et al., 2021).

Harnessing and sharing digital data assets could be improved by the development of an integrated data management system (i.e., dashboard) that could offer a singular place where property managers, turfgrass practitioners, and agronomists can merge data from disparate sources and more effectively predict the impact of site-specific management choices (Figure 5). To date, no singular software service provider has been able to universally address the demands of an integrated, client facing dashboard management tool, although progress is being made by several organizations.

Figure 5. A potential vision of an integrated digital data hub, universally associating digital datasets within a singular, user-facing dashboard.

Determining thresholds for triggering various treatments such as irrigation or pesticide applications are critical to management in turfgrass. However, thresholds using spectral or thermal data are difficult to develop across species, soils, and environmental conditions (Barbedo, 2019). This is, in part, because the degree of detected stress is relative, and non-stressed reference areas may be needed for comparison purposes. Vegetation or thermal indices (e.g., NDVI, CWSI; Table 1) may be more robust than single spectral waveband or canopy temperature measurements alone in indicating stress (e.g., drought), with thresholds that could be calibrated for a given site and species (e.g., genetic color, texture) (Sullivan and Holbrook, 2007; Bremer et al., 2011a). Still, at present, ground truthing is needed to confirm the cause(s) of plant stress (e.g., drought vs disease or multiple stressors). For example, NDVI has been related to N deficiency, salt stress, drought stress, and insect damage (Baghzouz et al., 2006; Bell et al., 2009; Johnsen et al., 2009; Xiang et al., 2017; Badzmierowski et al., 2019; Groover and Lawrence, 2020).

A rapidly growing field is crop spraying with sUAS, which can utilize remote sensing maps to target specific areas infested with weeds, disease, insects, etc. This strategy may eventually provide effective control with reduced pesticide application amounts, but additional research is required in turfgrass (Koo et al., 2021). Autonomous flights are also becoming increasingly important and may become the standard, but attention to public safety and adherence to regulations are important considerations (van der Merwe et al., 2020). Detailed discussions of these and other topics are beyond the scope of this chapter, but it is expected that the use of sUAS will have novel and broad impacts on turfgrass science and management.

7 Where to look for further information

1. van der Merwe, D., Burchfield, D. R., Witt, T. D., Price, K. P., and Sharda, A. (2020). Chapter One—Drones in agriculture. In D. L. Sparks (Ed.), Advances in Agronomy (Vol. 162, pp. 1–30). Academic Press. https://doi.org/10.1016/bs.agron.2020.03.001

2. Code of Federal Regulations – Part 107, Small Unmanned Aircraft Systems. (https://www.ecfr.gov/current/title-14/chapter-I/subchapter-F/part-107)

3. Kansas State University – Unmanned Aircraft Systems Program. See “Resources” tab for latest free information for UAS pilots: https://www.salina.k-state.edu/research-training/applied-aviation-research-center/

8 References

Aboutalebi, M., Allen, N., Torres-Rua, A. F., McKee, M. and Coopmans, C. (2019), Estimation of soil moisture at different soil levels using machine learning techniques and unmanned aerial vehicle (UAV) multispectral imagery, In J. A. Thomasson, M. McKee and R. J. Moorhead (Eds.), *Autonomous Air and Ground Sensing Systems for Agricultural Optimization and Phenotyping IV*, Vol. 11008, pp. 26, SPIE. https://doi.org/10.1117/12.2519743

Alvarez, G., Sevostianova, E., Serena, M., Sallenave, R. and Leinauer, B. (2016), Surfactant and polymer-coated sand effects on deficit irrigated bermudagrass turf, *Agron. J.* 108: 2245–2255. https://doi.org/10.2134/agronj2016.06.0329

An, N., Goldsby, A. L., Price, K. P. and Bremer, D. J. (2015), Using hyperspectral radiometry to predict green leaf area index of turfgrass, *Int. J. Remote Sens.* 36:1470-1483.

Assmann, J. J., Kerby, J. T., Cunliffe, A. M. and Myers-Smith, I. H. (2018), Vegetation monitoring using multispectral sensors – best practices and lessons learned from high latitudes, *J. Unmanned Veh. Sys*. 7: 54-75.

Bach, A., Bremer, D., Lavis, C. and Keeley, S. (2022a), Effects of drip irrigation and cultivation methods on establishment of seeded tall fescue, *Crop, Forage & Turfgrass Manage.* 8:1-10. https://doi.org/10.1002/cft2.20154

Bach, A. P., Bremer, D. J., Lavis, C. C. and Keeley, S. J. (2022b), Establishing seeded tall fescue with covers and drip irrigation methods, *Int. Turfgrass Soc. Res. J.* 1–9. https://doi.org/10.1002/its2.95

Badzmierowski, M. J., McCall, D. S. and Evanylo, G. (2019), Using hyperspectral and multispectral indices to detect water stress for an urban turfgrass system, *Agronomy* 9(8): 439.

Baghzouz, M., Devitt, D. A. and Morris, R. L. (2006), Evaluating temporal variability in the spectral reflectance response of annual ryegrass to changes in nitrogen applications and leaching fractions, *Int. J. Remote Sens.* 27(19): 4137–4157. https://doi.org/10.1080/01431160600851843

Baghzouz, M., Devitt, D. A. and Morris, R. L. (2007), Assessing canopy spectral reflectance of hybrid bermudagrass under various combinations of nitrogen and water treatments, *Applied Engineering in Agriculture* 23(6): 763–774. https://doi.org/10.13031/2013.24055

Barbedo, J. (2019), A review on the use of unmanned aerial vehicles and imaging sensors for monitoring and assessing plant stresses, *Drones* 3(2): 40. https://doi.org/10.3390/drones3020040

Bell, G. E., Howell, B. M., Johnson, G. V., Raun, W. R., Solie, J. B. and Stone, M. L. (2004), Optical sensing of turfgrass chlorophyll content and tissue nitrogen, *HortScience* 39(5): 1130–1132.

Bell, G. E., Martin, D. L., Koh, K. and Han, H. R. (2009), Comparison of turfgrass visual quality ratings with ratings determined using a handheld optical sensor, *HortTechnology* 19(2): 309–316.

Bell, G.E., Martin, D.L., Wiese, S.G., Dobson, D.D., Smith, M.W., Stone, M.L., & Solie, J.B. (2002), Vehicle-mounted optical sensing: An objective means for evaluating turf quality. *Crop Sci.* 42: 197–201.

Bock, C. H., Poole, G. H., Parker, P. E. and Gottwald, T. R. (2010), Plant disease severity estimated visually, by digital photography and image analysis, and by hyperspectral imaging, *Critical reviews in plant sciences* 29(2): 59-107.

Boon M.A., Drijfhout A.P. and Tesfamichael, S. (2017), Comparison of a fixed-wing and multi-rotor uav for environmental mapping applications: A case study. The International Archives of Photogrammetry, *Remote Sensing and Spatial Information Sciences* 42:47.

Booth, JC, McCall, DS, Sullivan, D, Askew, SA, Kochersberger, K. 2021. Investigating targeted spring dead spot management via aerial mapping and precision-guided fungicide applications. *Crop Science*, 61: 3134– 3144. https://doi-org.er.lib.k-state.edu/10.1002/csc2.20623

Bremer, D. J. and Ham, J. M. (1999), Effect of spring burning on the surface energy balance in a tallgrass prairie, *Agric. For. Meteorol*. 97:43-54.

Bremer, D.J., L.M. Auen, J.M. Ham, and C.E. Owensby. (2001), Evapotranspiration in a prairie ecosystem: Effect of grazing by cattle. *Agron. J.* 93: 338-348.

Bremer, D. J., Lee, H., Su, K. and Keeley, S. J. (2011a), Relationships between normalized difference vegetation index and visual quality in cool-season turfgrass: I. Variation among species and cultivars, *Crop Sci.* 51(5): 2212–2218. https://doi.org/10.2135/cropsci2010.12.0728

Bremer, D. J., Lee, H., Su, K. and Keeley, S. J. (2011b), Relationships between normalized difference vegetation index and visual quality in cool-season turfgrass: II. Factors affecting NDVI and its component reflectances, *Crop Sci*. 51(5): 2219–2227.

Cai G., Dias J. and Seneviratne, L. (2014), A survey of small scale unmanned aerial vehicles: Recent advances and future development trends, *Unmanned Systems* 2:175-199.

Campbell, J.B. 1996. Introduction to remote sensing. Second Edition. The Gilford Press, New York, NY.

Campbell, C. L. and Noe, J. P. (1985), The spatial analysis of soilborne pathogens and root diseases, *Annual review of phytopathology* 23(1): 129-148.

Caturegli, L., Corniglia, M., Gaetani, M., et al. (2016), Unmanned aerial vehicle to estimate nitrogen status of turfgrasses, *PLOS ONE* 11(6): e0158268. https://doi.org/10.1371/journal.pone.0158268

Caturegli, L., Gaetani, M., Volterrani, M., et al. (2019), Normalized Difference Vegetation Index versus Dark Green Colour Index to estimate nitrogen status on bermudagrass hybrid and tall fescue, *Int. J. Remote Sens.* 41(2): 455–470. https://doi.org/10.1080/01431161.2019.1641762

Caturegli, L., Matteoli, S., Gaetani, M., et al. (2020), Effects of water stress on spectral reflectance of bermudagrass, *Scientific Reports* 10(1): 15055. https://doi.org/10.1038/s41598-020-72006-6

Chandel, A. K., Khot, L. R., Molaei, B., Peters, R. T., Stöckle, C. O. and Jacoby, P. W. (2021), High-resolution spatiotemporal water use mapping of surface and direct-root-zone drip-irrigated grapevines using uas-based thermal and multispectral remote sensing, *Remote Sensing* 13(5): 954. https://doi.org/10.3390/rs13050954

Chandel, A. K., Molaei, B., Khot, L. R., Peters, R. T. and Stöckle, C. O. (2020), High resolution geospatial evapotranspiration mapping of irrigated field crops using multispectral and thermal infrared imagery with METRIC energy balance model, *Drones* 4(3): 52. https://doi.org/10.3390/drones4030052

Chávez, J. L., Torres-Rua, A. F., Woldt, et al. (2020), A decade of unmanned aerial systems in irrigated agriculture in the western U.S., *Applied Engineering in Agriculture* 36(4): 423–436. https://doi.org/10.13031/aea.13941

Dao, P. D., He, Y. and Proctor, C. (2021), Plant drought impact detection using ultra-high spatial resolution hyperspectral images and machine learning, *International Journal of Applied Earth Observation and Geoinformation* 102: 102364. https://doi.org/10.1016/j.jag.2021.102364

Deery, D., Jimenez-Berni, J., Jones, H., Sirault, X. and Furbank, R. (2014), Proximal remote sensing buggies and potential applications for field-based phenotyping, *Agronomy* 4: 349−79 doi: 10.3390/agronomy4030349

Delvapour, N., Koparan, C., Nowatzki, J., Bajwa, S. and Sun, X. (2021), A technical study on UAV characteristics for precision agriculture applications and associated practical challenges, *Remote Sens*. 13: 1204.

Diaz, M. D. C. and Peck, D. C. (2007), Overwintering of annual bluegrass weevils, *Listronotus maculicollis*, in the golf course landscape, *Entomologia experimentalis et applicate*. 125(3): 259-268.

Dyer, D.W. (2022), Integrating canopy dynamics, soil moisture, and soil physical properties to improve irrigation scheduling in turfgrass systems [Ph.D. dissertation]. Kansas State Univ.

Emekli, Y., Bastug, R., Buyuktas, D. and Emekli, N. Y. (2007), Evaluation of a crop water stress index for irrigation scheduling of bermudagrass, *Agricultural water management* 90(3): 205-212.

Fahlgren, N., Gehan, M.A. and Baxter, I. (2015), Lights, camera, action: high-throughput plant phenotyping is ready for a close-up, *Current opinion in plant biology* 24: 93−99 doi: 10.1016/j.pbi.2015.02.006

Feng, L., Chen, S., Zhang, C., Zhang, Y. and He, Y. (2021), A comprehensive review on recent applications of unmanned aerial vehicle remote sensing with various sensors for high-throughput plant phenotyping, *Computers and Electronics in Agriculture* 182:106033 doi: 10.1016/j.compag.2021.106033.

Fenstermaker-Shaulis, L. K., Leskys A. and Devitt, D. A. (1997), Utilization of remotely sensed data to map and evaluate turfgrass stress associated with drought, *J. Turfgrass Manag.* 2: 65–81. doi:10.1300/J099v02n01_06

Friell, J. and Straw, C. (2021), Comparing ground-based and aerial data at field scale during dry down on golf course fairways, *Int. Turf. Soc. Res. J.* pp. 1-8. https://doi.org/10.1002/its2.46

Gago, J., Douthe, C., Coopman, R. E., et al. (2015), UAVs challenge to assess water stress for sustainable agriculture, *Agricultural Water Management*, 153: 9–19. https://doi.org/10.1016/J.AGWAT.2015.01.020

Gireesh, M., Rijal, J. P. and Joseph, S. V. (2021), Spatial distribution of hunting billbugs (Coleoptera: Curculionidae) in sod farms, *Insects*, 12(5): 402.

Gitelson, A. A., Kaufman, Y. J., Stark, R. and Rundquist, D. (2002), Novel algorithms for remote estimation of vegetation fraction. *Remote Sens. of Environ.* 80(1): 76-87.

Gitelson, A. A., Keydan, G. P. and Merzlyak, M. N. (2006), Three-band model for noninvasive estimation of chlorophyll, carotenoids, and anthocyanin contents in higher plant leaves, *Geophys. Res. Lett*. 33: 111402 doi:10.1029/2006Gl026457

Green, D. E., Burpee, L. L. and Stevenson, K. L. (1998), Canopy reflectance as a measure of disease in tall fescue, *Crop Sci*. 38(6): 1603-1613.

Groover, W. L. and Lawrence, K. S. (2020), Plant health evaluations of *Belonolaimus longicaudatus* and *Meloidogyne incognita* colonized bermudagrass using remote sensing, *Journal of Nematology* 52: 2020–2109. https://doi.org/10.21307/JOFNEM-2020-109

Haghverdi, A., Reiter, M., Singh, A. and Sapkota, A. (2021), Hybrid Bermudagrass and Tall Fescue Turfgrass Irrigation in Central California: II. Assessment of NDVI, CWSI, and Canopy Temperature Dynamics, *Agronomy* 11(9): 1733.

Han, L., Yang, G., Dai, H., Yang, H., et al. (2019), Combining self-organizing maps and biplot analysis to preselect maize phenotypic components based on UAV high-throughput phenotyping platform, *Plant Methods* 15(1). doi: 10.1186/s13007-019-0444-6.

Hatfield, J. L, Gitelson, A. A., Schepers, J. S. and Walthall, C. L. (2008), Application of spectral remote sensing for agronomic decisions, *Agron J.* 100: S-117-S-131.

Henderson, C. A. (2021), Identification of disease stress in turfgrass canopies using thermal imagery and automated aerial image analysis. [M.S. thesis]. Virginia Tech.

Henderson, C. A. and McCall, D. S. (2021), Methods for Estimating Dollar Spot at Varying Altitudes of Aerial Imagery [Abstract], *ASA, CSSA, SSSA International Annual Meeting*, Salt Lake City, UT. https://scisoc.confex.com/scisoc/2021am/meetingapp.cgi/Paper/134083

Henry, G. M., Burton, M. G. and Yelverton, F. H. (2009), Heterogeneous distribution of weedy Paspalum species and edaphic variables in turfgrass, *HortScience* 44(2): 447-451.

Holman, F., A. Riche, A. Michalski, et al. (2016), High throughput field phenotyping of wheat plant height and growth rate in field plot trials using UAV based remote sensing, *Remote Sens*. 8(12): 1031. doi: 10.3390/rs8121031.

Hong, M., Bremer, D. J. and van der Merwe, D. (2019a), Thermal imaging detects early drought stress in turfgrass utilizing small unmanned aircraft systems, *Agrosystems, Geosciences & Environment* 2(1): 1–9. https://doi.org/10.2134/age2019.04.0028

Hong, M., Bremer, D. J. and van der Merwe, D. (2019b), Using small unmanned aircraft systems for early detection of drought stress in turfgrass, *Crop Sci*. 59(6): 2829–2844. https://doi.org/10.2135/cropsci2019.04.0212

Horst, G. L., Engelke, M. C. and Meyers, W. (1984), Assessment of visual evaluation techniques, *Agron. J*. 76(4): 619–622. doi: 10.2134/agronj1984.00021962007600040027x.

Horvath, B. J., Kravchenko, A. N., Robertson, G. P. and Vargas Jr, J. M. (2007), Geostatistical analysis of dollar spot epidemics occurring on a mixed sward of creeping bentgrass and annual bluegrass, *Crop Sci*. 47(3): 1206-1216.

Hutchens, W. J., Goatley, J. M., Kerns, J. P., Nita, M., Straw, C. M., Sullivan, D., Henderson, C. A. and McCall, D. S. (2021), Environmental and Edaphic Factors That Influence Spring Dead Spot Epidemics, *ASA, CSSA, SSSA International Annual Meeting*, Salt Lake City, UT. https://scisoc.confex.com/scisoc/2021am/meetingapp.cgi/Paper/134068

Islam, M. S., Studer, B., Møller, I. M. and Asp, T. (2014), Genetics and biology of cytoplasmic male sterility and its applications in forage and turf grass breeding, *Plant Breed*. 133(3). doi: 10.1111/pbr.12155.

Jiang, Y. and Carrow, R. N. (2005), Assessment of narrow-band canopy spectral reflectance and turfgrass performance under drought stress, *HortScience* 40(1): 242–245. https://doi.org/10.21273/HORTSCI.40.1.242

Jiang, Y. and Carrow, R. N. (2007), Broadband spectral reflectance models of turfgrass species and cultivars to drought stress, *Crop Sci*. 47(4): 1611–1618.

Johnsen, A. R., Horgan, B. P., Hulke, B. S. and Cline, V. (2009), Evaluation of remote sensing to measure plant stress in creeping bentgrass (*Agrostis stolonifera* L.) Fairways, *Crop Sci*. 49(6): 2261–2274. https://doi.org/10.2135/cropsci2008.09.0544

Karcher, D. E. and Richardson, M. D. (2013), Digital image analysis in turfgrass research, In *Turfgrass: Biology, use, and management*, pp. 1133–1149.

Koo, D., Goncalves, C. G. and Askew, S. D. (2021), Influence of height and speed on spray deposition pattern of an agricultural spray drone, *ASA, CSSA, SSSA International Annual Meeting*, Salt Lake City, UT. https://scisoc.confex.com/scisoc/2021am/meetingapp.cgi/Paper/139240

Lee, H., Bremer, D. J., Su, K. and Keeley, S. J. (2011), Relationships between normalized difference vegetation index and visual quality in turfgrasses: Effects of mowing height, *Crop Sci*. 51: 323-332. doi:10.2135/cropsci2010.05.0296

Li, F., Piasecki, C., Millwood, R. J., Wolfe, B., Mazarei, M. and Stewart, C. N. (2020), High-Throughput Switchgrass Phenotyping and Biomass Modeling by UAV, *Front. Plant Sci*. 11. doi: 10.3389/fpls.2020.574073.

Li, L., Zhang, Q. and Huang D. (2014), A review of imaging techniques for plant phenotyping, *Sensors* 11: 20078-111.

Marín, J., Yousfi, S., Mauri, P. V., Parra, L., Lloret, J. and Masaguer, A. (2020), RGB vegetation indices, NDVI, and biomass as indicators to evaluate C3 and C4 turfgrass under different water conditions, *Sustainability* (Switzerland) 12(6): 2160. https://doi.org/10.3390/su12062160

Mauri, P. V., Parra, L., Yousfi, S., Lloret, J. and Marin, J. F. (2021), Evaluating the effects of environmental conditions on sensed parameters for green areas monitoring and smart irrigation systems, *Sensors* 21(6): 2255. https://doi.org/10.3390/s21062255

McCall, D. S., Zhang, X., Sullivan, D. G., Askew, S. D. and Ervin, E. H. (2017), Enhanced soil moisture assessment using narrowband reflectance vegetation indices in creeping bentgrass, *Crop Sci*. 57(S1): S-161.

McCall, D. S., Sullivan, D. G., Zhang, X., Martin, S. B., Wong, A. and Ervin, E. H. (2021), Influence of synthetic phthalocyanine pigments on light reflectance of creeping bentgrass, *Crop Sci*. 6*1*(1): 804-813.

Patton, A., Volenec, J. and Reicher, Z. (2007), Stolon growth and dry matter partitioning explain differences in zoysiagrass establishment rates, *Crop Sci*. 47(3): 1237–1245.

Peñuelas, J., Filella, I., Biel, C., Serrano, L. and Save, R. (1993), The reflectance at the 950–970 nm region as an indicator of plant water status, *Int. J. Remote Sens. 14*(10): 1887-1905.

Peterson, K. W., Bremer, D. J. and Blonquist Jr, J. M. (2017), Estimating transpiration from turfgrass using stomatal conductance values derived from infrared thermometry, *Int. Turf. Soc. Res. J*. 13: 113-118. doi: 10.2134/itsrj2016.09.0788

R Core Team (2021), R: A language and environment for statistical computing, R Foundation for Statistical Computing, Vienna, Austria. URL https://www.R-project.org/.

Richardson, M. D., Karcher, D. E. and Purcell, L. C. (2001), Quantifying turfgrass cover using digital image analysis, *Crop Sci*. 41(6): 1884–1888. doi: 10.2135/cropsci2001.1884.

Ritchie, G. L. and Bednardz, C. W. (2005), Estimating defoliation of two distinct cotton types using reflectance data, *J. Cotton Sci*. 9:182–188.

Roberson, T. L., Badzmierowski, M. J., Stewart, R. D., Ervin, E. H., Askew, S. D. and McCall, D. S. (2021), Improving soil moisture assessment of turfgrass systems utilizing field radiometry, *Agronomy 11*(10): 1960.

Rockstad, G., Austin, R., Yu, X., et al. (2020), Evaluation of UAV-based imagery for drought stress traits in St. Augustinegrass, *ASA, CSSA and SSSA annual meeting*.

Rouse, J.W., Haas Jr., R. H., Schell, J. A. and Deering, D. W. (1974), Monitoring vegetation systems in the Great Plains with ERTS., *Proc. ERTS-1 Symp.*, 3rd, NASA, Washington, DC, pp. 309–317.

Sangha, H. S., Sharda, A., Koch, L., Prabhakar, P. and Wang, G. (2020), Impact of camera focal length and sUAS flying altitude on spatial crop canopy temperature evaluation, *Computers and Electronics in Agriculture* 172: 105344. https://doi.org/10.1016/j.compag.2020.105344

Spurlock, T. N. (2009), Epidemiology and etiology of zoysiagrass diseases in Northwest Arkansas, University of Arkansas.

Steinke, K., Chalmers, D., Thomas, J., White, R. and Fipps, G. (2010), Drought response and recovery characteristics of St. Augustinegrass cultivars, *Crop Sci*. 50(5): 2076.

Straw, C., Friell, J. and Horgan, B. (2019), Precision irrigation for golf courses using sensor and mapping technologies, *ASA-CSSA-SSSA Annual Meeting*. http://conservancy.umn.edu/handle/11299/214353

Sullivan, D. G. and Holbrook, C.C. (2007), Using ground-based reflectance measurements as a selection criteria for drought- and aflatoxin- resistant peanut genotypes. *Crop Sci*. 47: 1040-1050.

Sullivan, D. G., Shaw, J. N., Mask, P. L., Rickman, D., Luvall J. and Wersinger, J. M. (2004), Evaluating corn nitrogen variability via remote-sensed data, *Commun. in Soil Sci. Plant Anal*. 35: 2465-2483.

Sullivan, D. G., Fulton, J. P., Shaw, J. N. and Bland. G. (2007), Evaluating the sensitivity of an unmanned thermal infrared aerial system to detect water stress in a cotton canopy, *Trans. ASABE* 50: 1955-1962.

Suplick-Ploense, M. R., Alshammary, S. F. and Qian, Y. L. (2011), Spectral reflectance response of three turfgrasses to leaf dehydration, *Asian Journal of Plant Sciences* 10(1): 67–73. https://doi.org/10.3923/ajps.2011.67.73

Taghvaeian, S., Chávez, J., Hattendorf, M. and Crookston, M. (2013), Optical and thermal remote sensing of turfgrass quality, water stress, and water use under different soil and irrigation treatments, *Remote Sensing* 5(5): 2327–2347. https://doi.org/10.3390/rs5052327

Tattaris, M., Reynolds, M. P. and Chapman, S. C. (2016), A direct comparison of remote sensing approaches for high-throughput phenotyping in plant breeding, *Front. Plant Sci*. 7: 1131. doi: 10.3389/fpls.2016.01131.

Thamm, H. P., Brieger N., Neitzke K. P., Meyer M., Jansen R. and Mönninghof, M. (2015), SONGBIRD-an innovative UAS combining the advantages of fixed wing and multi rotor UAS. International Archives of the Photogrammetry, *Remote Sensing & Spatial Information Sciences* 40: 345-249

Tmušić, G., Manfreda, S., Aasen, H., et al. (2020), Current practices in UAS-based environmental monitoring, *Remote Sensing* 12(6): 1001. https://doi.org/10.3390/rs12061001

Trappe, J. M., Karcher, D. E., Richardson, M. D. and Patton, A. J. (2011a), Bermudagrass and Zoysiagrass Cultivar Selection: Part 1, Clipping Yield, Scalping Tendency, and Golf Ball Lie, *Appl. Turfgrass Sci*. 8(1). doi: 10.1094/ats-2011-0630-01-rs.

Trappe, J. M., Karcher, D. E., Richardson, M. D. and Patton, A. J. (2011b), Bermudagrass and Zoysiagrass Cultivar Selection: Part 2, Divot Recovery, *Appl. Turfgrass Sci*. 8(1). doi: 10.1094/ats-2011-0630-02-rs.

Tucker, C. J. (1979), Red and photographic infrared linear combinations for monitoring vegetation, *Remote Sens. Environ*. 8:127–150

van der Merwe, D., Burchfield, D. R., Witt, T. D., Price, K. P. and Sharda, A. (2020), Chapter One—Drones in agriculture, In D. L. Sparks (Ed.), *Advances in Agronomy*, Academic Press, Vol. 162, pp. 1–30. https://doi.org/10.1016/bs.agron.2020.03.001

van der Merwe, D., Skabelund, L. R., Sharda, A., Blackmore, P. and Bremer, D. (2017), Towards characterizing green roof vegetation using color-infrared and thermal sensors, *Cities Alive 15th Annual Green Roof and Wall Conference,* Seattle, WA, pp. 18– 21.

Van Rossum, G., and F. L. Drake. (2011), The Python language reference manual. Bristol, U.K.: Network Theory Ltd.

Wang, T., A. Chandra, J. Jung, and A. Chang. (2022), UAV remote sensing based estimation of green cover during turfgrass establishment. *Comput. Electron. Agric.* 194: 106721

Wei, X., Aguilera, M., Walcheck, R., Tholl, D., Li, S., Langston Jr, D. B. and Mehl, H. L. (2021), Detection of soilborne disease utilizing sensor technologies: Lessons learned from studies on stem rot of peanut, *Plant Health Progress* PHP-03.

Wherley, B. B. G., Skulkaew, P., Chandra, A., Genovesi, A. D. and Engelke, M. C. (2011), Low-input performance of zoysiagrass (Zoysia spp.) cultivars maintained under dense tree shade, *HortScience* 46(7): 1033–1037.

Wilber, A. L., Czarnecki, J.M. P., & McCurdy, J. D. (2021). An ArcGIS Pro workflow to extract vegetation indices from aerial imagery of small plot turfgrass research. *Crop Sci.* 62: 503–511. https://doi.org/10.1002/csc2.20669

Xiang, M., Moss, J. Q., Martin, D. L., Su, K., Dunn, B. L. and Wu, Y. (2017), Evaluating the salinity tolerance of clonal-type bermudagrass cultivars and an experimental selection, *HortScience* 52(1): 185–191. https://doi.org/10.21273/HORTSCI10773-16

Yang, G., Liu, J., Zhao, C., et al. (2017), Unmanned aerial vehicle remote sensing for field-based crop phenotyping: Current status and perspectives, *Front. Plant Sci*. 8. doi: 10.3389/fpls.2017.01111.

Yucky, E.D.D., Putrada, A.G., and Abdurohman, M. (2021), IoT drone camera for a paddy crop health detector with RGB comparison, *2021 9th International Conference on Information and Communication Technology (ICoICT)*, 2021, pp. 155-159, doi: 10.1109/ICoICT52021.2021.9527421.

Zarco-Tejada, P. J., González-Dugo, V. and Berni, J. A. J. (2012), Fluorescence, temperature and narrow-band indices acquired from a UAV platform for water stress detection using a micro-hyperspectral imager and a thermal camera, *Remote Sens. Environ.* 117: 322–337. https://doi.org/10.1016/j.rse.2011.10.007

Zhang, J., Poudel, B., Kenworthy, K. E., et al. (2018), Drought responses of above-ground and below-ground characteristics in warm-season turfgrass, *J. Agron. Crop Sci*. 205(1): 1-12. doi: 10.1111/jac.12301.

Zhang, J., Schwartz, B. M., Maleski, J., et al. (2019a), Application of Unmanned Serial Systems based imagery and data analytics in turfgrass field trials, *ASA, CSSA and SSSA annual meeting*.

Zhang, J., Virk, S., Porter, W., Kenworthy, K., Sullivan, D. and Schwartz, B. (2019b), Applications of unmanned aerial vehicle based imagery in turfgrass field trials, *Front. Plant Sci*. 10: 593. https://doi.org/10.3389/fpls.2019.00279

Zhang J, Maleski, J., Jespersen, D., Waltz Jr, F.C., Rains, G. and Schwartz, B. (2021), Unmanned aerial system-based weed mapping in sod production using a convolutional neural network, *Front. Plant Sci.* 12: 702626. doi: 10.3389/fpls.2021.702626

Zhang, Y. and Zhang, N. (2018), Imaging technologies for plant high-throughput phenotyping: a review, *Frontiers of Agricultural Science and Engineering* 5: 406−19 doi: 10.15302/j-fase-2018242